



1 Investigation of the wet removal rate of black carbon in East 2 Asia: validation of a below- and in-cloud wet removal scheme in 3 FLEXPART v10.4

4 Yongjoo Choi¹, Yugo Kanaya¹, Masayuki Takigawa¹, Chunmao Zhu¹, Seung-Myung Park², Atsushi
5 Matsuki³, Yasuhiro Sadanaga⁴, Sang-Woo Kim⁵, Xiaole Pan⁶, Ignacio Pissó⁷

6 ¹ Research Institute for Global Change, Japan Agency for Marine-Earth Science and Technology (JAMSTEC), Yokohama,
7 2360001, Japan

8 ² Division of Climate & Air Quality Research, National Institute of Environmental Research, Kyungseo-dong, Seo-Gu, Incheon
9 404170, Korea

10 ³ Institute of Nature and Environmental Technology, Kanazawa University, Kanazawa 9201192, Japan

11 ⁴ Department of Applied Chemistry, Graduate School of Engineering, Osaka Prefecture University, 1-1 Gakuen-cho, Naka-
12 ku, Sakai, Osaka 5998531, Japan

13 ⁵ School of Earth and Environmental Sciences, Seoul National University, Seoul 08826, Korea

14 ⁶ Institute of Atmospheric Physics, Chinese Academy of Sciences, Beijing, China

15 ⁷ NILU – Norwegian Institute for Air Research, Kjeller 2027, Norway

16 Correspondence to: Yongjoo Choi (choingjoo@jamstec.go.jp)

17 Abstract

18 Understanding the global distribution of atmospheric black carbon (BC) is essential to unveil its climatic effect. However,
19 there are still large uncertainties regarding the simulation of BC transport due to inadequate information about the removal
20 process. We accessed the wet removal rate of BC in East Asia based on long-term measurements over the 2010–2016 period
21 at three representative background sites (Baengnyeong and Gosan in South Korea and Noto in Japan). The average wet removal
22 rate, represented by transport efficiency (TE), i.e. the fraction of undeposited BC particles during transport, was estimated as
23 0.73 in East Asia from 2010 to 2016. According to accumulated precipitation along trajectory, TE was lower in East and North
24 China, where the industrial sector (thin-coated) is dominant; in contrast, that in South Korea and Japan showed higher values
25 due to the transport sector (thick-coated), with emissions mainly from diesel vehicles. By the same token, TE in winter and
26 summer showed the highest and lowest values, respectively, depending on the dominant emission sectors, such as house heating
27 (thick-coated) and industry. The average half-life and e -folding lifetime of BC were 2.8 and 7.1 days, respectively, similar to
28 previous studies, but those values differed according to the geographical location and meteorological conditions of each site.
29 Next, by comparing TE from the FLEXible PARTicle (FLEXPART) Lagrangian transport model (version 10.4), we diagnosed
30 the scavenging coefficients (s^{-1}) of the below- and in-cloud scavenging scheme implemented in FLEXPART. The overall
31 median TE from FLEXPART (0.91) was overestimated compared to the measured value, implying underestimation of wet
32 scavenging coefficients in the model simulation. The median of the below-cloud scavenging coefficient showed a lower value
33 than that calculated from FLEXPART, by a factor of 1.7. On the other hand, the overall median of the FLEXPART in-cloud
34 scavenging coefficients was highly underestimated by 1 order of magnitude compared to the measured value. From the analysis
35 of artificial neural networks, the convective available potential energy, which is well known as an indicator of vertical
36 instability, should be considered in the in-cloud scavenging process to improve the representative regional difference in BC
37 wet scavenging over East Asia. For the first time, this study suggested an effective and straightforward evaluation method for
38 wet scavenging schemes (both below- and in-cloud) by introducing TE along with excluding effects from the inaccurate
39 emission inventories.



40 1. Introduction

41 Black carbon (BC) is the most significant light-absorbing aerosol that can cause positive radiative forcing on climate change
42 (Winiger et al., 2016; Myhre et al., 2013; Bond et al., 2013; Emerson et al., 2018). However, state-of-the-art models still have
43 a limitation in evaluating the direct radiative forcing of BC because of the large model uncertainties in simulating BC
44 concentrations (Xu et al., 2019; Bond et al., 2013; Samset et al., 2014; Wang et al., 2014a). This can partly be attributed to the
45 following three reasons: inaccurate bottom-up emission inventory, the complexity of BC hygroscopicity, and an imprecise
46 dry/wet deposition scheme. First, because BC is mainly contributed by scattered emission sources, the uncertainty of BC
47 emission rates is large compared to other species whose emissions are dominated by large sources (Zheng et al., 2018). Second,
48 BC itself is hydrophobic immediately after emission, is subsequently converted to possessing hydrophilic properties through
49 the aging process and transportation (Moteki et al., 2007; Matsui et al., 2018), and finally acts as cloud condensation nuclei
50 (Kuwata et al., 2007; Bond et al., 2013). Third, while BC particles are transported in the atmosphere, they can be removed by
51 dry and/or wet deposition, including below-cloud (i.e., washout) and in-cloud (i.e., rainout) processes. Wet deposition is still
52 challenging to predict BC concentration in the atmosphere due to the difficulties of accurate evaluation of wet removal
53 (Emerson et al., 2018; Bond et al., 2013; Lee et al., 2013). Specifically, the in-cloud process is more efficient and complicated
54 than the below-cloud process because the nucleation removal of aerosol particles within clouds is thought to account for more
55 than 50% of the aerosol particle mass removal from the atmosphere globally (Grythe et al., 2017; Textor et al., 2006).

56 Accompanied with the refinement of BC emission inventories over East Asia (Choi et al., 2020; Kanaya et al., 2016), wet
57 removal rates have been one of the main topics to better predict BC behavior by using the term transport efficiency (TE), which
58 is the fraction of undeposited BC particles during transport, because TE has been proven to be a good proxy for wet scavenging.
59 Moteki et al. (2012), which was further elaborated from Oshima et al. (2012), reported the first observational evidence of the
60 size-dependent activation of BC removal over the Yellow Sea during the Aerosol Radiative Forcing in East Asia (A-FORCE)
61 airborne measurement campaign in the spring of 2009. Kondo et al. (2016) demonstrated an altitude dependence, with typical
62 decreasing size distributions at higher altitudes associated with wet removal from A-FORCE in winter 2013. Kanaya et al.
63 (2016) elucidated the relationship between the wet removal rate of BC and accumulated precipitation along trajectory (APT)
64 from long-term measurements (2009–2015) at Fukue, Japan. Miyakawa et al. (2017) reported the effects of BC aging related
65 to in-cloud scavenging during transport on the alteration of the BC size distribution and mixing stats during the spring of 2015
66 at the same location. Matsui et al. (2013) demonstrated that the difference in the coating thickness of BC particles depended
67 on the growing process (condensation and coagulation), indicating that the coagulation process is necessary to produce thickly
68 coated BC particles that are preferentially removed via the wet scavenging process. Recently, numerous fine mode particles,
69 including BC from polluted areas scavenging in clouds were more pronounced in East Asia, not only at a local scale but also
70 at a large regional scale (Liu et al., 2018), because high aerosol loading conditions are usually associated with significant cloud
71 cover (Eck et al., 2018).

72 BC and carbon monoxide (CO) are byproducts of the incomplete combustion of carbon-based fuels, and the ratio between
73 ΔBC (the difference from the baseline level) and ΔCO could be a useful parameter for characterizing combustion types.
74 Adopting APT, a useful index for the strength of wet deposition (Kanaya et al., 2016; Kanaya et al., 2019), the magnitude of
75 the BC wet removal rate according to precipitation can be easily characterized by TE. Although some previous studies have
76 investigated wet scavenging schemes in models (Grythe et al., 2017; Croft et al., 2010), those results may include bias due to
77 the effect of inaccurate emission rate because emission rates and deposition terms were not necessarily separated. For the first



78 time, the emission and deposition terms are distinctly separated in this study by introducing TE; this allows for the wet
79 scavenging scheme to be evaluated more accurately. By elaborating the regional $\Delta BC/\Delta CO$ ratio (Choi et al., 2020), this study
80 investigates the characteristics of the BC wet removal rate over East Asia using long-term measurements (more than 3 years)
81 with the best effort to acquire reliable BC concentrations with wide spatial coverages over East Asia. The differences in wet
82 removal rates depending on measurement sites and administrative districts (and season) are discussed in Sections 3.1 and 3.2,
83 respectively. Afterward, to evaluate the representativeness of the scavenging scheme in the recently updated FLEXible
84 PARTicle dispersion model (FLEXPART) version 10.4, the wet scavenging coefficients for below- and in-cloud processing
85 were estimated from the wet removal rate by allocating the air mass location (such as below or within the cloud) and
86 meteorological variables along the pathway of air mass transport.

87 2. Methods

88 2.1 Measurement sites and instruments

89 To investigate wet removal rates of the outflow air mass from China and Korea peninsula, BC and CO data from three
90 measurement sites (Baengnyeong, Gosan in Korea and Noto in Japan; Figure 1a) were carefully selected for this study by
91 considering major emission sources near the measurement sites and by obtaining reliable BC concentrations from different
92 instruments. As detailed information on the measurement sites and instruments is described in Choi et al. (2020), we only
93 address brief information here. Baengnyeong (124.63°E, 37.97°N), one of the intensive measurement stations operated by the
94 Korean Ministry of Environment, is frequently affected by airmasses from China (East, North, and Northeast) and North Korea.
95 Gosan (126.17°E, 33.28°N) is located in the southern part of Korea and is frequently affected by airmasses from East China
96 and South Korea. BC and CO were also measured at the Noto Ground-based Research Observatory (NOTOGRO, 137.36°E,
97 37.45°N), located on the Noto Peninsula on the western coast of Japan, which is frequently affected by airmasses from
98 Northeast China and Japan. The measurement periods were mainly in the early 2010s but slightly different depending on the
99 sites (Figure S1). The longest measurement period was in Noto for approximately 6 years (from 2011 to 2016), followed by
100 that in Baengnyeong (5 years) and Gosan (3 years).

101 As the best effort to obtain reliable BC concentrations from different instruments, only well-validated instruments were used
102 in this study. Hourly $PM_{2.5}$ elemental carbon (EC) was measured by a Sunset EC/OC analyzer with optical correction for
103 Baengnyeong. Multi-angle absorption photometer (MAAP 5012) was used to measure hourly BC in $PM_{2.5}$ for Noto. At Gosan,
104 BC in PM_{1} was monitored by a continuous light absorption photometer (CLAP) with three wavelengths including 467, 528,
105 and 652 nm and the absorption was corrected following Bond (1999). At Noto, an improved mass absorption efficiency (MAE)
106 of $10.3 \text{ m}^2 \text{ g}^{-1}$ instead of the default value ($6.6 \text{ m}^2 \text{ g}^{-1}$) was applied to estimate the BC mass concentration, as suggested based
107 on calibrations using the thermal/optical method and the laser-induced incandescence technique (Kanaya et al., 2013; Kanaya
108 et al., 2016). CLAP also showed a good correlation with co-located $PM_{2.5}$ EC concentration from the Sunset EC/OC analyzer
109 and the best-fitted line was close to one (1.17), similar or slightly lower than the range of reported uncertainty, ~25% (Ogren
110 et al., 2017). Hourly CO concentrations were measured by a gas filter correlation CO analyzer (Model 300 EU Teledyne Inc.)
111 at Baengnyeong and by a nondispersive infrared absorption photometer (48C, Thermo Scientific) at the other two sites. The
112 overall uncertainty of BC and CO measurements from different instruments was estimated to be less than 15% (except for
113 Gosan; 20%) and 5%, respectively, which leads to 10% uncertainty of overall regional $\Delta BC/\Delta CO$ ratio (Choi et al., 2020).



114 2.2 Backward trajectory and meteorological data

115 To identify the air mass origin region, 72 h backward trajectories were calculated four times a day (00, 06, 12, 18 UTC) using
116 the Hybrid Single Particle Lagrangian Integrated Trajectory (HYSPPLIT) Model version 4 (Draxler et al., 2018). The starting
117 altitude was 500 m above ground level (AGL). Notably, we used the European Centre for Medium-Range Weather Forecasts
118 (ECMWF) ERA5, which provides a much finer resolution of $0.25^\circ \times 0.25^\circ$, as inputs for HYSPLIT instead of Global Data
119 Assimilation System (GDAS) $1^\circ \times 1^\circ$ data with 23 pressure levels to improve the accurate assessment of air mass transportation
120 pathways and to acquire more detailed information on meteorological conditions. According to the pathway of air mass
121 transportation, the detailed meteorological information for precipitation and clouds was acquired from ERA5 hourly data on
122 both single and pressure levels (37 levels; 1000 hPa to 1 hPa) to identify the below- and/or in-cloud cases and to calculate the
123 wet scavenging coefficients.

124 If precipitation occurred before the air mass arrived at the main BC source region, it is difficult to investigate the wet removal
125 effect because the effects of precipitation could be underestimated at receptor sites. Therefore, we considered the residence
126 time (Li et al., 2014; Ashbaugh et al., 1985) of each grid cell ($0.25^\circ \times 0.25^\circ$) and the BC emission rates (mass/time) from the
127 Regional Emission inventory in ASia (REAS; Figure 1a) emission inventory (Kurokawa et al., 2013) version 2.1 to identify
128 the potential emission region by multiplying residence time and emission rates. First, when the air mass altitude was lower than
129 2.5 km, the air mass velocities (V_n and V_{n+1}) were calculated by distances from the central point in a target grid cell to two-way
130 endpoints of backward trajectories (D_n and D_{n+1}) using $V_n = D_n / \Delta t$ and $V_{n+1} = D_{n+1} / \Delta t$ (Figure 1b). Here, Δt and n are the time
131 interval of meteorological data (1 h) and n th grid cell, respectively. Then, by assuming the air mass velocity is constant within
132 the time interval, the residence time in a grid cell (T_{grid}) was calculated by considering both the distance of each grid corner
133 (d_n and d_{n+1}) and the corresponding velocities (V_n and V_{n+1}) using $d_n / V_n + d_{n+1} / V_{n+1}$. Based on the identified potential emission
134 region, APT was calculated only after the air mass passed through the potential emission region when precipitation occurred.
135 Figure 1c reveals the geographical distribution for the mean BC mass of identified potential emission regions, indicating that
136 this approach was appropriate because of good spatial coverage over East Asia, including East China, a major emission source
137 for BC.

138 2.3 Transport efficiency (TE)

139 The TE of BC is defined as the ratio of the BC and CO concentrations measured at the receptor site to that anticipated if
140 there was no wet removal during transport (i.e., APT is zero). Thus, the TE of the air mass was calculated by eq. (1),

$$141 \quad TE = \frac{[\Delta BC / \Delta CO]_{APT > 0}}{[\Delta BC / \Delta CO]_{APT = 0}} \quad (1)$$

142 where delta (Δ) indicates the difference between BC and CO concentrations and their baseline concentrations (Moteki et al.,
143 2012; Oshima et al., 2012; Kanaya et al., 2016). The baseline CO was estimated as a 14-day moving 5th percentile from the
144 observed CO mixing ratio, but the BC baseline was regarded as zero because the atmospheric lifetime of BC is known as
145 several days, which is much shorter than that of CO (1–2 months). $[\Delta BC / \Delta CO]_{APT = 0}$ indicated the regional median value of
146 $\Delta BC / \Delta CO$ under dry conditions implying the original emission ratio. In our previous work, we successfully elucidated that
147 $[\Delta BC / \Delta CO]_{APT = 0}$ depends on the regional characteristics of the energy consumption types (Kanaya et al., 2016; Choi et al.,
148 2020). The decrease of the ratio with APT, $[\Delta BC / \Delta CO]_{APT > 0}$, was related to BC-specific removal due to wet scavenging
149 processes and thus the TE was effective indicator to investigate the wet removal process. Although TE is also affected by dry



150 deposition, but the effect of dry deposition could be negligible because dry deposition velocities were much lower than the
151 default setting in the global models (Choi et al., 2020).

152 2.4 FLEXPART model

153 To compare the wet removal rates between the model simulation and measured values, the FLEXPART v10.4 was used to
154 simulate BC wet scavenging over East Asia using the backward mode. Detailed information for the FLEXPART is readily
155 found in the literature (e.g., Stohl et al., 2005); thus, we only briefly describe the information here. The FLEXPART version
156 10.4 was the official version to allow turning on the wet scavenging module in the backward simulation mode
157 (<https://www.flexpart.eu/downloads>, obtained 10 October 2019). The equation and detailed description for the below- and in-
158 cloud scavenging scheme are explained in Pisso et al. (2019) and Grythe et al. (2017). The FLEXPART model was executed
159 with operational reanalysis meteorological data from the ECMWF ERA-Interim at a spatial resolution of $1^\circ \times 1^\circ$ with 60 full
160 vertical levels. Temporally, ECMWF has a resolution of 3 h, with 6 h analysis and 3 h forecast time steps. The period and
161 daily frequency of simulation were the same as those of the HYSPLIT model (past 72 h and four times, respectively). It should
162 be noted that chemistry and microphysics could not be resolved by the FLEXPART. The FLEXPART model, therefore, ignores
163 the aging process (from hydrophobic to hydrophilic state changes and size changes of BC) and assumes that all BC particles
164 are aged hydrophilic particles. The logarithmic size distribution of BC with a mean diameter of $0.16 \mu\text{m}$ and a standard
165 deviation of 1.84, in accordance with measurement in Japan, was used (Miyakawa et al., 2017). A total of 10^4 particles were
166 randomly released at 500 m from each receptor site during 1 h when the measurement data were existed. To validate the wet
167 scavenging scheme in FLEXPART by comparison with the measured TE value, the wet scavenging coefficients for below- and
168 in-clouds were extracted from FLEXPART to calculate TE.

169 3 Results

170 3.1 Overall variation of transport efficiency (TE)

171 Figure 2 shows that measured $[\Delta\text{BC}/\Delta\text{CO}]_{\text{APT}=0}$ (left panel) and TE variations (right panel) depend on APT and the
172 measurement sites. The overall median $[\Delta\text{BC}/\Delta\text{CO}]_{\text{APT}=0}$ was $6.4 \text{ ng m}^{-3} \text{ ppb}^{-1}$, which converged from Baengnyeong (6.2 ng
173 $\text{m}^{-3} \text{ ppb}^{-1}$), Gosan ($6.5 \text{ ng m}^{-3} \text{ ppb}^{-1}$) and Noto ($6.7 \text{ ng m}^{-3} \text{ ppb}^{-1}$), indicating that TE is characterized with a regional
174 $[\Delta\text{BC}/\Delta\text{CO}]_{\text{APT}=0}$ per site. We divided APT into 9 range bins and applied exponential fitting equations to quantify the wet
175 removal process. Among $N_{\text{APT}>0}$ (total number of data points when $\text{APT} > 0 \text{ mm}$), only the data point fraction in each bin to
176 $N_{\text{APT}>0} \geq 2\%$ was considered to secure the statistic. It should be noted that we found the relationship between TE and APT by
177 using the stretched exponential decay (SED) equation, $\exp(-A_1 \times \text{APT}^{A_2})$, instead of the widely used equation, $A-$
178 $B \times \log(\text{APT})$, because the coefficients of determination (R^2) was improved up to 0.981 though TE values from three sites were
179 used (Table 1). This fitting equation is normally used to describe below-cloud scavenging, whereas wet removal of BC is
180 generally believed to be dominated by in-cloud rather than below-cloud processes because of the small size of BC-containing
181 particles. Therefore, the equations should contain both below- and in-cloud scavenging effects. The parameters A_1 ($0.269 \pm$
182 0.039) and A_2 (0.385 ± 0.035) of the overall fitting were higher and lower, respectively, than the derived equation from the
183 Fukue site ($A_1 = 0.109$ and $A_2 = 0.68$) (Kanaya et al., 2016). It can be easily deduced that the wet removal effect at the three
184 sites was initially more effective than that at Fukue, but the wet removal effect at Fukue gradually accelerated as the APT
185 increased. In particular, the A_2 value is important for calculating the TE of BC for long-range transport, e.g., toward the Arctic



186 (Kanaya et al., 2016; Zhu et al., 2019), because A_2 determines the magnitude of the wet removal efficiency according to APT.
187 Thus, the newly obtained SED equation indicates that more BC will be transported to the Arctic region than previously reported.

188 The decreasing pattern of median TE for Baengnyeong did not closely follow the overall SED and had a much lower R^2
189 (0.77), indicating that the wet removal process at Baengnyeong could not simply be expressed by APT. In contrast, the R^2 of
190 Gosan and Noto were sufficiently high to represent the wet removal characteristics. The aging process due to different traveling
191 times might be one of the reasons. Because long-range transported BC has a larger core diameter than BC from local sources
192 (Lamb et al., 2018; Ueda et al., 2016), these larger BC cores are preferentially removed via the wet scavenging process (Moteki
193 et al., 2012). However, previous studies reported that the mass median diameter (MMD) of BC at Baengnyeong, Gosan, and
194 Noto in spring were 218, 196, and 200 nm (Oh et al., 2015; Ueda et al., 2016; Oh et al., 2014), respectively, indicating much
195 more aging compared with local emissions in Seoul, South Korea (180 nm) and Tokyo, Japan (163 nm) (Park et al., 2019;
196 Ohata et al., 2019). Moreover, there were no significant differences in the mean traveling times for the air mass (when APT >
197 0) arriving at the three sites (37.9, 39.0, and 37.8 h for Baengnyeong, Gosan, and Noto, respectively), indicating that the
198 difference in the level of the BC aging process might be negligible.

199 The difference in the wet removal rate among measurement sites could be partly explained by the difference in meteorology.
200 The monthly mean meteorological parameters indicated that Baengnyeong has characteristics of low precipitation (80.6 mm),
201 cloud cover (0.57), total column cloud water (0.06 kg m⁻²), and high cloud bottom height (2.5 km) compared to other sites,
202 suggesting the lower exposure time to both below- and/or in-cloud condition during the transportation (Figure 3). In contrast,
203 the SED fittings for both Gosan and Noto showed similar ranges of high precipitation (127 and 174 mm), total cloud cover
204 (0.65 and 0.64), and total column cloud water (0.09 and 0.12 kg m⁻²) but low cloud bottom height (1.9 and 2.0 km), respectively.
205 In addition, the different BC coating thicknesses according to the emission source and fuel types could also contribute to the
206 site difference of the wet removal rate, which will be further discussed in section 3.2.

207 Using the overall SED fitting equation, TE at 0.5 (TE=0.5) and e -folding (TE=1/ e) could be reached when the APT values
208 were 11.7 and 30.2 mm, respectively (Table 1). Similar to the SED results, Baengnyeong needed much higher precipitation of
209 70.9 and 202 mm to reach TE=0.5 and TE=1/ e , respectively, but the other sites showed lower APTs of 16.4 mm and 42.3 mm
210 for Gosan and 8.0 mm and 20.3 mm for Noto, respectively. Considering the annual mean precipitation at the three sites (1542
211 mm), it took 2.8 and 7.1 days to reach TE=0.5 and TE=1/ e , respectively. Kanaya et al. (2016) reported a similar half-life and
212 shorter e -folding lifetime for BC at Fukue (2.3 ± 1.0 and 4.0 ± 1.0 days, respectively), calculated from the 15.0 ± 3.2 mm and
213 25.5 ± 6.1 mm of APT to reach TE=0.5 and TE=1/ e , respectively, along with annual precipitation (2335 mm). This calculated
214 e -folding lifetime in East Asia was much shorter than 16.0 days for the global model (Grythe et al., 2017).

215 Based on a similar approach over the Yellow Sea using an aircraft-borne single particle soot photometer (SP2) during the
216 A-FORCE campaign (Oshima et al., 2012), attaining TE=0.5 required different magnitudes of APT depending on not only the
217 air mass origin but also the altitude. These authors also reported that the TE of northern China was higher than that of southern
218 China regardless of altitude. Therefore, in the next section, we will further investigate why the difference in halving or e -
219 folding lifetimes depends on region and season by analyzing the difference in the origin of air masses and the seasonal variation
220 of BC emission sources.

221 3.2 Regional and seasonal variations of the transport efficiency (TE)

222 Figure 4 indicates the variation of TE depending on the potential source regions (hereafter regions) and seasons. The R^2 for



223 each source region was varied from 0.656 to 0.945 and was lower in East and North China and North Korea and higher in
224 other regions (Table 1). A similar tendency of R^2 , $TE=0.5$ also showed different APTs, i.e., higher in East and North China and
225 lower in other regions. The regional difference in wet removal efficiency can partly be attributed to the following reasons.

226 First, the transport pathway of air masses from East and North China could be less exposed to in-cloud scavenging than other
227 regions because the most of potential emission source in East and North China is located over 30°N (Figure 1c), which has
228 low cloud cover and water contents along with high cloud bottom heights (Figure 3). Although the amount of APT was similar
229 to other regions, it was mostly composed of below-cloud scavenging, therefore, the wet removal efficiency should be lower
230 than the dominant in-cloud scavenging region. Second, the difference in the coating thickness of BC particles, depending on
231 the emission sectors, could be a major factor causing the difference in the wet removal efficiency because thickly-coated BC
232 particles are much easier to remove by wet scavenging than less coated and/or freshly emitted BC (Miyakawa et al., 2017).
233 Typically, BC emitted from industrial regions, transport from diesel vehicles, and domestic sectors has characteristics of weakly,
234 moderate, and strongly coated BC, respectively (Han et al., 2019; Liu et al., 2019), based on insignificant differences in the
235 MMD of BC from those emission sectors (190 – 200 nm). This result coincided with the major emission sector of the REAS
236 emission inventory in East and North China and North Korea (~57.5% emitted from industrial sectors) compared to other sites
237 (12% – 39%). In contrast, Northeast China showed low APT for reaching $TE=0.5$ and $TE=1/e$ because the dominant BC
238 emission sector was residential sector (48.3%) which has a thickly coated characteristic. BC from South Korea and Japan
239 reached $TE=0.5$ and $TE=1/e$ with a small amount of APT because moderately coated BC was mostly emitted from the transport
240 sector (73.4%), mainly from diesel vehicles. It should be noted that the dominant emission sectors of industry (for East and
241 North China and North Korea) or transport sectors (South Korea and Japan) were also confirmed by the Emission Database
242 for Global Atmospheric Research (EDGAR) in 2010 and MIX in 2010 (Li et al., 2017; Crippa et al., 2018).

243 In case of seasonal variation in TE, the decreasing magnitude of TE was obviously emphasized in fall and winter, which
244 was much steeper than that in spring and summer (Figure 4b). This tendency was reflected in the effect of the residential sector,
245 which has thickly coated BC, which increased due to house heating as the temperature decreased. In contrast to winter, the
246 APT for reaching $TE=0.5$ in spring and summer was the highest among the seasons. This might be caused by the increasing
247 fraction of BC from the industrial sector in China while decreasing emissions from residential sectors (Kurokawa et al., 2013).

248 3.3 Comparison of measured and FLEXPART-simulated TE

249 In this section, by extracting the wet scavenging coefficients (Λ ; s^{-1}) from the FLEXPART simulation, the difference in TE
250 between the measured and simulated values was investigated. The scavenging coefficient (Λ ; s^{-1}) is defined as the rate of
251 aerosol washout and/or rainout due to the wet removal process. The TE value based on measurements and FLEXPART can be
252 expressed by multiplying each TE ($1 - \text{removal rate}$) of serial grid cells as in eq. (2),

$$253 \quad TE = (1 - \eta_1)(1 - \eta_2) \cdots (1 - \eta_n) \quad (2)$$

254 where η_n indicates the removal rate in the n th grid cell and is expressed as eq. (3),

$$255 \quad \eta = [1 - \exp(-\Lambda \cdot t)] \cdot f_g \quad (3)$$

256 where t and f_g indicate the residence time and fraction for the subgrid in a grid cell, respectively. Because the precipitation is
257 not uniform in a single grid cell, f_g accounts for the variability of precipitation in a grid cell in FLEXPART. f_g is a function of



258 large-scale and convective precipitation, as described in Stohl et al. (2005). Although the grid resolution of the input
259 meteorological data for the HYSPLIT model ($0.25^\circ \times 0.25^\circ$) is much finer than that for FLEXPART ($1^\circ \times 1^\circ$), we assumed the
260 same potential emission region as the HYSPLIT model for calculating TE because there was no significant difference in the
261 air mass pathway between the two outputs.

262 The overall median value of measured TE was 0.72, and Baengnyeong showed the highest (0.88), followed by Gosan (0.70)
263 and Noto (0.68) due to reasons explained in the previous sections. In comparison, the overall median value of FLEXPART TE
264 (0.91) was much higher than the measured TE, indicating that the wet scavenging coefficients in the FLEXPART scheme were
265 significantly underestimated. Moreover, the difference in FLEXPART TE depending on the measurement sites (0.95 for
266 Baengnyeong, 0.94 for Gosan, and 0.87 for Noto) was not large as the measured TE, suggesting that the regional difference in
267 meteorological variables was relatively normalized and that the influence of other variables, which were not considered in the
268 wet scavenging scheme, might be excluded in the calculation. Meanwhile, it is difficult to capture the local variation from
269 coarse grid sizes, despite the air mass transport pathway between the two models being similar, because the key variables for
270 determining the wet scavenging coefficient (such as precipitation and cloud cover) could have a large local variability. In
271 addition, this approach still had a limitation in determining whether the overestimation of TE was resulting from the below- or
272 in-cloud scavenging processes. Nevertheless, with similar rationale, further comparison of measured and simulated scavenging
273 processes would provide information to better represent wet removal schemes.

274 3.4 Below-cloud scavenging efficiency (Λ_{below})

275 From this section, we aimed to investigate the below- and in-cloud scavenging in detail by discriminating the representative
276 cases according to cloud information from the ERA5 pressure level data to overcome the limitation of the local variability of
277 meteorological input variables. By considering the vertical height of the air mass from the HYSPLIT model and cloud
278 information from ERA5, we successfully distinguished the dominant cases for below-cloud (no residence time within the cloud)
279 and in-cloud (no residence time below the cloud) cases when precipitation $\geq 0.01 \text{ mm hr}^{-1}$. The median TE and residence time
280 for only in-cloud cases (0.72 and $\sim 7,200 \text{ h}$) were much lower and longer, respectively, than those for only below-cloud cases
281 (0.89 and $\sim 5,100 \text{ h}$), indicating that most BC particles were effectively removed via the in-cloud scavenging process (Table 2).
282 In the case of below-cloud scavenging, the deviation of TE from unity could be simply converted to the scavenging coefficient
283 (Λ_{below}) by considering the precipitation intensity, raindrop size, aerosol size, and residence time in a grid cell. Because many
284 studies have made an effort to parameterize Λ_{below} using observation data and/or the theoretical calculation (Xu et al., 2017;
285 Wang et al., 2014b; Feng, 2007), we also parameterized this coefficient using a simplified method by following the scheme of
286 below-cloud scavenging in FLEXPART v10.4 (Laakso et al., 2003), which only considers the precipitation rate and aerosol
287 size. Assuming a BC size $\sim 200 \text{ nm}$, TE for below-cloud can be expressed using equations (2) and (3) by substituting Λ with
288 Λ_{below} , which depends only on the precipitation rate in the subgrid cell (I_{total} ; the ratio of precipitation to f_g). Because Λ_{below} can
289 be determined by constraining the proportion to the summation of I_{total} , hourly Λ_{below} from the sequential grid cell in a single
290 case can easily be obtained by minimizing χ^2 , $(\text{TE}_{\text{measured}} - \text{TE}_{\text{calculated}})^2$ when $\chi^2 < 0.1$. This was conducted using an R function,
291 optimization (optim; <https://stat.ethz.ch/R-manual/R-devel/library/stats/html/optim.html>), included in the standard R package
292 “stats”.

293 Figure 5a indicates the empirical cumulative density function for the measured Λ_{below} from 869 cases. Although a substantial
294 fraction of Λ_{below} was close to zero (or negative), the median Λ_{below} was significantly different from zero and also positive
295 ($7.9 \times 10^{-6} \text{ s}^{-1}$), with an interquartile range of $-1.7 \times 10^{-5} \text{ s}^{-1}$ to $5.3 \times 10^{-5} \text{ s}^{-1}$. Negative Λ_{below} values have been reported in previous



296 studies (Laakso et al., 2003; Pryor et al., 2016; Zikova and Zdimal, 2016); therefore, we assumed that these negative values
297 reflected the uncertainty in measurements and/or inclusion of BC, which might be continuously supplemented in airmasses.
298 As the threshold of I_{total} increased from 0.01 (all cases) to 0.2 mm hr⁻¹ (median), Λ_{below} values were increased by a factor of 2.5
299 to $2.0 \times 10^{-5} \text{ s}^{-1}$ ($-2.5 \times 10^{-5} \text{ s}^{-1}$ to $9.0 \times 10^{-5} \text{ s}^{-1}$). Using these obvious increasing tendencies of Λ_{below} according to I_{total} , we
300 determined the empirical fitting equation by investigating the relationship between median Λ_{below} and each bin of I_{total} . Figure
301 5b indicates Λ_{below} as a function of I_{total} by allocation to 11 logarithmic bins. As the estimated I_{total} bins covered the I_{total} ranges,
302 0.03 to 2.0 mm hr⁻¹ (5th percentile to 95th percentile), this exponential fitting equation ($A \times I_{\text{total}}^B$) could be representative for
303 below-cloud scavenging over East Asia. The constant A and exponent B with a 95% confidence interval were 2.0×10^{-5} (1.9
304 $- 2.2 \times 10^{-5}$) and 0.54 (0.46 – 0.64), respectively. Instead of the SED equation shown in Figure 2, we chose the exponential
305 fitting equation because of its higher R² (0.973) compared to that from SED fitting (0.903), as well as being widely used in
306 previous studies.

307 Figure 6 shows the comparison of Λ_{below} from reported values with this study by assuming that the BC size was
308 approximately 200 nm. To compare the measured Λ_{below} , we used mean fractional bias (MFB; $2 \times [A - B] / [A + B]$), where A and
309 B denote Λ_{below} of reported values and this study, respectively. Our newly measured Λ_{below} values were located in the
310 intermediate range of reported Λ_{below} , and the mean deviations between measured and all reported values were relatively
311 constant with increasing I_{total} because the mean absolute MFBs were slightly increased from 1.4 to 1.6. It should be noted that
312 Λ_{below} from Laakso et al. (2003), which is the default scheme for below-cloud scavenging in the FLEXPART model version
313 10 or higher (Grythe et al., 2017), showed fairly good agreement with our Λ_{below} among the reported values (mean absolute
314 MFBs was 0.68). MFB was positive at low I_{total} , but the tendency was opposite based on $I_{\text{total}} \sim 0.1 \text{ mm hr}^{-1}$, suggesting that
315 Λ_{below} might be converged within a similar range when we consider the range of I_{total} . Although Λ_{below} from Laakso et al. (2003)
316 showed good agreement with our results, the median Λ_{below} ($6.6 \times 10^{-6} \text{ s}^{-1}$) was overestimated compared to our estimation (4.0
317 $\times 10^{-6} \text{ s}^{-1}$), by a factor of 1.7 when we recalculated the only below-cloud cases. The MFBs from other schemes were too high
318 or low to declare reasonable results. For example, the Λ_{below} of secondary ions in Beijing (Xu et al., 2017) had the highest MFB
319 (1.68), and although the diameter ranges were larger ($\sim 500 \text{ nm}$) than those of BC, the effect of differences in diameter might
320 be negligible.

321 3.5 In-cloud scavenging coefficient (Λ_{in})

322 Compared to Λ_{below} , the calculation of Λ_{in} is much more complicated because many factors can influence the in-cloud
323 scavenging process, such as precipitation, total cloud cover (TCC), the specific cloud total water content (CTWC) and so on.
324 The detailed description for the complicated equation for Λ_{in} in FLEXPART v10 is presented in Grythe et al. (2017), and the
325 equation for Λ_{in} can be simply expressed as follows:

$$326 \quad \Lambda_{\text{in}} = \frac{i_{\text{cr}} \cdot F_{\text{nuc}} \cdot I_{\text{total}} \cdot TCC}{CTWC \cdot f_g} \quad (4)$$

327 where i_{cr} and F_{nuc} are the cloud water replenishment factor (6.2; default value) and the nucleation efficiency, respectively. It
328 should be mentioned that Λ_{in} was calculated by following the FLEXPART scheme using the ERA5 meteorological data
329 ($0.25^\circ \times 0.25^\circ$) instead of the FLEXPART simulation ($1^\circ \times 1^\circ$) to match the grid size of the input data with the HYSPLIT backward
330 trajectory. Among the 769 cases for in-cloud cases, equations (2) and (3) were also used to calculate TE for only in-cloud cases
331 by substituting Λ with calculated Λ_{in} . Unlike the hourly measured Λ_{below} calculated by optimization, the only overall median



332 Λ_{in} (Λ_{in}^*) for in-cloud cases was calculated using equation (3) because Λ_{in} cannot be constrained by a specific variable.

333 The FLEXPART Λ_{in}^* ($7.28 \times 10^{-6} \text{ s}^{-1}$) was underestimated by 1 order of magnitude compared to our estimated Λ_{in}^* ($8.06 \times$
334 10^{-5} s^{-1}). When TE from FLEXPART for in-cloud cases (all cases) was recalculated by considering a ten (five) times higher
335 Λ_{in} , the median TE was 0.73 (0.79), which was much close to the measured TE (0.72). Although the grid size of input
336 meteorological data for two approaches did not match, the underestimation of the in-cloud scavenging scheme in FLEXPART
337 was confirmed. Grythe et al. (2017) reported an overestimation of observed BC (a factor of 1.68) due to the inaccurate emission
338 source rather than the underestimated in-cloud removal efficiencies. Although the effect of BC particle dispersion to adjacent
339 grid cells was neglected in our approach, the underestimation of in-cloud scavenging coefficients was obvious because the
340 accuracy of the emission inventory did not affect the estimated Λ_{in}^* . Looking more closely into the sites, the FLEXPART Λ_{in}^*
341 at Noto was remarkably underestimated by 1 order of magnitude, followed by Gosan (~90%) and Baengnyeong (~43%),
342 similar to the order of the wet removal efficiency. It should be noted that the coefficient of variation (CV; standard deviation
343 divided by the mean) of FLEXPART Λ_{in}^* was much lower (0.23) than the measured Λ_{in}^* (0.78), indicating that FLEXPART
344 Λ_{in}^* did not accurately represent the actual regional difference in the real world. Among the input meteorological variables in
345 equation (4), the CV of I_{total} was the highest as 0.22, which was similar to the CV of FLEXPART Λ_{in}^* , followed by CTWC
346 (0.08), f_g (0.03), and TCC (0.02), suggesting that the difference in FLEXPART Λ_{in}^* could be partially explained by I_{total} rather
347 than other variables. Among the meteorological variables that were not considered in equation (4), the convective available
348 potential energy (CAPE), which is well known as an indicator of vertical instability (Mori et al., 2014), had the highest CV of
349 0.31.

350 We employed an artificial neural network (ANN) method to compare the importance of CAPE with other considered input
351 meteorological variables for determining the hourly Λ_{in} , not Λ_{in}^* . We applied a stricter selection for in-cloud cases that only
352 when in-cloud scavenging occurred less than three times (i.e., three cells) in a single case, regardless of the number of below-
353 cloud occurrences. Because the effect of below-cloud scavenging was successfully excluded from the TE using the derived
354 equation for Λ_{below} in the previous section, the Λ_{in} in less than three in-cloud cases can also be calculated by optimization based
355 on the remaining TE. We applied a threshold of three cases here because the number of data (230 cases) was sufficient to
356 conduct statistical analysis, while the optimization uncertainty could be reduced to its minimum. The ANN model was trained
357 using the six meteorological variables (CAPE, CTWC, f_g , F_{nuc} , I_{total} , and TCC), and all variables were normalized by the
358 minimum and maximum of each variable ($[x-\min(x)]/[\max(x)-\min(x)]$). To determine optimal node numbers in the hidden
359 layer, we applied a ‘caret’ package of the R function that contain several sets of machine learning modes and validation tools
360 (<https://cran.r-project.org/web/packages/caret/caret.pdf>) and adopted a method from the ‘neuralnet’ package that is fit for a
361 multi-hidden layer. By varying the ‘size’ (node number) from 5 to 20 and using k -fold cross validation, the selected cases were
362 randomly divided 3:1 into training (172 data points) and validation data (58 data points). Garson’s algorithm in the
363 “NeuralNetTools” package was used to identify the relative importance of six input variables in the final neural network
364 (Garson, 1991). The model’s performance was assessed in these independent validation data by calculating the root mean
365 squared error. The optimal number of nodes in the hidden layer was 12 (Figure 7a).

366 Figure 7b shows the relative importance of input variables for calculating Λ_{in} using Garson’s algorithm. The most important
367 input variable was CAPE, with a value of 35%, followed by CTWC, I_{total} , and so on, confirming that CAPE should be
368 considered in the Λ_{in} calculation. Typically, enhancing wet removal by convective clouds successfully reduces the aloft BC
369 concentration in the free troposphere (Koch et al., 2009). Therefore, convective process is important in tropical regions but has



370 a slightly lower impact at mid-latitudes (Luo et al., 2019; Grythe et al., 2017; Xu et al., 2019). Moreover, previous studies
371 pointed out convective scavenging to be a key parameter in determining the BC concentration in model simulation (Lund et
372 al., 2017; Xu et al., 2019) and the role of wet removal by convective clouds might be significant when most airmasses travel
373 above the planetary boundary layer. Unfortunately, the current version of FLEXPART does not implement convective
374 scavenging (Philipp and Seibert, 2018), which could be a plausible reason for the underestimation of FLEXPART Λ_{in} . Although
375 the relative importance of each variable cannot be parameterized to calculate Λ_{in} , this approach highlights that CAPE is one
376 of the key factors for determining Λ_{in} over East Asia. In the future, more information might be required to evaluate the in-
377 cloud scavenging scheme using Weather Research and Forecasting (WRF)-FLEXPART at a higher resolution in further studies,
378 since a 0.25° grid size is still not sufficient to reproduce convective clouds (typically 10 km or less).

379 4 Conclusions

380 The wet removal rates and scavenging coefficients for BC were investigated by the term of $\Delta BC/\Delta CO$ ratios from long-
381 term, best-effort observations at three remote sites in East Asia (Baengnyeong and Gosan in South Korea and Noto in Japan).
382 Combined with backward trajectories covering the past 72 h, accumulated precipitation along trajectories (APT), and transport
383 efficiency (TE; $[\Delta BC/\Delta CO]_{APT>0}/[\Delta BC/\Delta CO]_{APT=0}$), the assessment of BC wet removal efficiency was conducted as an aspect
384 of the pathway of trajectories, including the successful identification of below- and in-cloud cases. The overall wet removal
385 rates as a function of APT, the half-life and *e*-folding lifetime were similar to those of previous studies but showed large
386 regional differences depending on the measurement sites. The difference in the wet removal rate, depending on the
387 measurement site, can be explained by the different meteorological conditions, such as the precipitation rate, cloud cover, total
388 column cloud water, and cloud bottom height. Moreover, the difference in regional or seasonal wet removal rates could be
389 explained by the different coating thicknesses according to the BC emission sources (thin- and thick-coated BC from the
390 industrial and residential sectors, respectively) because the thick-coated BC particles are preferentially removed due to cloud
391 processes. By discriminating below- and in-cloud dominant cases according to cloud vertical information from ERA5 pressure
392 level data, scavenging coefficients for below-cloud (Λ_{below}) and in-cloud (Λ_{in}^*) were simply converted from the measured TE
393 values. The Λ_{below} from the FLEXPART scheme was overestimated by a factor of 1.7 compared to the measured Λ_{below} , although
394 the measured Λ_{below} showed good agreement with the below-cloud scheme in FLEXPART among the reported scavenging
395 coefficients. In contrast to Λ_{below} , FLEXPART Λ_{in}^* was highly underestimated by 1 order of magnitude compared to measured
396 Λ_{in}^* , suggesting that the current in-cloud scavenging scheme did not represent regional variability. By diagnosing the relative
397 importance of the input variables using the artificial neuron network (ANN) method, we found that the convective available
398 potential energy (CAPE), which is an indicator of vertical instability, should be considered to improve the in-cloud scavenging
399 scheme because convective scavenging could be regarded as a key parameter for determining the accurate BC concentration
400 in a model. This study could contribute not only to improving the below-cloud scavenging scheme implemented in a model,
401 especially FLEXPART, but also to providing evidence for complementary in-cloud scavenging schemes by considering the
402 convective scavenging process. For the first time, these results suggest a novel and straightforward approach to evaluating the
403 wet scavenging scheme in various models and to enhancing the understanding of BC behavior by excluding the effect of
404 inaccurate emission inventory.



405 **Author contributions.**

406 YC and YK designed the study and prepared the paper, with contributions from all co-authors. YC, MT, and CZ optimized
407 the FLEXPART model and revised the paper. YC simulated the FLEXPART model and conducted analyses. SMP was
408 responsible for measurements at Baengnyeong. AM and YS conducted measurements at Noto, and SWK contributed to ground
409 observations and quality control at Gosan. XP and IP contributed to the data analysis. All co-authors provided professional
410 comments to improve the paper.

411 **Competing interests.**

412 The authors declare that they have no conflicts of interest.

413 **Code/Data availability.**

414 The observational data set for BC and CO are available upon request to the corresponding author.

415 **Acknowledgments.**

416 The authors thank NOAA ARL and ECMWF for providing the HYSPLIT model and ERA5 meteorological data.

417 **Financial support.**

418 This research has been supported by the Environment Research and Technology Development Fund of the Ministry of the
419 Environment, Japan (grant no. 2-1803).



References

- Andronache, C.: Estimated variability of below-cloud aerosol removal by rainfall for observed aerosol size distributions, *Atmos. Chem. Phys.*, 3, 131-143, 10.5194/acp-3-131-2003, 2003.
- Ashbaugh, L. L., Malm, W. C., and Sadeh, W. Z.: A residence time probability analysis of sulfur concentrations at grand Canyon National Park, *Atmos. Environ.*, 19, 1263-1270, [https://doi.org/10.1016/0004-6981\(85\)90256-2](https://doi.org/10.1016/0004-6981(85)90256-2), 1985.
- Baklanov, A., and Sorensen, J. H.: Parameterisation of radionuclide deposition in atmospheric long-range transport modelling, *Physics and Chemistry of the Earth, Part B: Hydrology, Oceans and Atmosphere*, 26, 787-799, [https://doi.org/10.1016/S1464-1909\(01\)00087-9](https://doi.org/10.1016/S1464-1909(01)00087-9), 2001.
- Bond, T. C., Doherty, S. J., Fahey, D., Forster, P., Berntsen, T., DeAngelo, B., Flanner, M., Ghan, S., Kärcher, B., and Koch, D.: Bounding the role of black carbon in the climate system: A scientific assessment, *J. Geophys. Res. Atmos.*, 118, 5380-5552, 2013.
- Choi, Y., Kanaya, Y., Park, S. M., Matsuki, A., Sadanaga, Y., Kim, S. W., Uno, I., Pan, X., Lee, M., Kim, H., and Jung, D. H.: Regional variability in black carbon and carbon monoxide ratio from long-term observations over East Asia: assessment of representativeness for black carbon (BC) and carbon monoxide (CO) emission inventories, *Atmos. Chem. Phys.*, 20, 83-98, 10.5194/acp-20-83-2020, 2020.
- Crippa, M., Guizzardi, D., Muntean, M., Schaaf, E., Dentener, F., van Aardenne, J. A., Monni, S., Doering, U., Olivier, J. G. J., Pagliari, V., and Janssens-Maenhout, G.: Gridded emissions of air pollutants for the period 1970–2012 within EDGAR v4.3.2, *Earth Syst. Sci. Data*, 10, 1987-2013, 10.5194/essd-10-1987-2018, 2018.
- Croft, B., Lohmann, U., Martin, R. V., Stier, P., Wurzler, S., Feichter, J., Hoose, C., Heikkilä, U., van Donkelaar, A., and Ferrachat, S.: Influences of in-cloud aerosol scavenging parameterizations on aerosol concentrations and wet deposition in ECHAM5-HAM, *Atmos. Chem. Phys.*, 10, 1511-1543, 10.5194/acp-10-1511-2010, 2010.
- Draxler, R., Stunder, B., Rolph, G., Stein, A., and Taylor, A.: HYSPLIT4 User's Guide Version 4-Last Revision: February 2018, HYSPLIT Air Resources Laboratory, MD, USA, 2018.
- Eck, T. F., Holben, B. N., Reid, J. S., Xian, P., Giles, D. M., Sinyuk, A., Smirnov, A., Schafer, J. S., Slutsker, I., Kim, J., Koo, J. H., Choi, M., Kim, K. C., Sano, I., Arola, A., Sayer, A. M., Levy, R. C., Munchak, L. A., O'Neill, N. T., Lyapustin, A., Hsu, N. C., Randles, C. A., Da Silva, A. M., Buchard, V., Govindaraju, R. C., Hyer, E., Crawford, J. H., Wang, P., and Xia, X.: Observations of the Interaction and Transport of Fine Mode Aerosols With Cloud and/or Fog in Northeast Asia From Aerosol Robotic Network and Satellite Remote Sensing, *Journal of Geophysical Research: Atmospheres*, 0, 10.1029/2018JD028313, 2018.
- Emerson, E. W., Katich, J. M., Schwarz, J. P., McMeeking, G. R., and Farmer, D. K.: Direct Measurements of Dry and Wet Deposition of Black Carbon Over a Grassland, *J. Geophys. Res. Atmos.*, 123, 212,277-212,290, 10.1029/2018JD028954, 2018.
- Feng, J.: A 3-mode parameterization of below-cloud scavenging of aerosols for use in atmospheric dispersion models, *Atmos. Environ.*, 41, 6808-6822, <https://doi.org/10.1016/j.atmosenv.2007.04.046>, 2007.
- Garson, G. D.: Interpreting neural-network connection weights, *Artif. Intell. Expert*, 6, 46–51, 1991.
- Grythe, H., Kristiansen, N. I., Groot Zwaafink, C. D., Eckhardt, S., Ström, J., Tunved, P., Krejci, R., and Stohl, A.: A new aerosol wet removal scheme for the Lagrangian particle model FLEXPART v10, *Geosci. Model Dev.*, 10, 1447-1466, 10.5194/gmd-10-1447-2017, 2017.
- Han, C., Li, S.-M., Liu, P., and Lee, P.: Size Dependence of the Physical Characteristics of Particles Containing Refractory Black Carbon in Diesel Vehicle Exhaust, *Environmental Science & Technology*, 53, 137-145, 10.1021/acs.est.8b04603, 2019.
- Jylhä, K.: Empirical scavenging coefficients of radioactive substances released from chernobyl, *Atmospheric Environment. Part A. General Topics*, 25, 263-270, [https://doi.org/10.1016/0960-1686\(91\)90297-K](https://doi.org/10.1016/0960-1686(91)90297-K), 1991.
- Kanaya, Y., Taketani, F., Komazaki, Y., Liu, X., Kondo, Y., Sahu, L. K., Irie, H., and Takashima, H.: Comparison of Black Carbon Mass Concentrations Observed by Multi-Angle Absorption Photometer (MAAP) and Continuous Soot-Monitoring System (COSMOS) on Fukue Island and in Tokyo, Japan, *Aerosol Sci. Technol.*, 47, 1-10, 10.1080/02786826.2012.716551, 2013.
- Kanaya, Y., Pan, X., Miyakawa, T., Komazaki, Y., Taketani, F., Uno, I., and Kondo, Y.: Long-term observations of black carbon mass concentrations at Fukue Island, western Japan, during 2009–2015: constraining wet removal rates and emission strengths from East Asia, *Atmos. Chem. Phys.*, 16, 10689-10705, 10.5194/acp-16-10689-2016, 2016.
- Kanaya, Y., Yamaji, K., Miyakawa, T., Taketani, F., Zhu, C., Choi, Y., Komazaki, Y., Ikeda, K., Kondo, Y., and Klimont, Z.: Rapid reduction of black carbon emissions from China: evidence from 2009-2019 observations on Fukue Island, Japan, *Atmos. Chem. Phys. Discuss.*, 2019, 1-28, 10.5194/acp-2019-1054, 2019.
- Koch, D., Schulz, M., Kinne, S., McNaughton, C., Spackman, J. R., Balkanski, Y., Bauer, S., Berntsen, T., Bond, T. C., Boucher, O., Chin, M., Clarke, A., De Luca, N., Dentener, F., Diehl, L., Dubovik, O., Easter, R., Fahey, D. W., Feichter, J., Fillmore, D., Freitag, S., Ghan, S., Ginoux, P., Gong, S., Horowitz, L., Iversen, T., Kirkev, aring, g. A., Klimont, Z., Kondo, Y., Krol,



- M., Liu, X., Miller, R., Montanaro, V., Moteki, N., Myhre, G., Penner, J. E., Perlwitz, J., Pitari, G., Reddy, S., Sahu, L., Sakamoto, H., Schuster, G., Schwarz, J. P., Seland, Ø., Stier, P., Takegawa, N., Takemura, T., Textor, C., van Aardenne, J. A., and Zhao, Y.: Evaluation of black carbon estimations in global aerosol models, *Atmos. Chem. Phys.*, 9, 9001-9026, 10.5194/acp-9-9001-2009, 2009.
- Kondo, Y., Moteki, N., Oshima, N., Ohata, S., Koike, M., Shibano, Y., Takegawa, N., and Kita, K.: Effects of wet deposition on the abundance and size distribution of black carbon in East Asia, *J. Geophys. Res. Atmos.*, 121, 4691-4712, 10.1002/2015JD024479, 2016.
- Kurokawa, J., Ohara, T., Morikawa, T., Hanayama, S., Janssens-Maenhout, G., Fukui, T., Kawashima, K., and Akimoto, H.: Emissions of air pollutants and greenhouse gases over Asian regions during 2000–2008: Regional Emission inventory in ASia (REAS) version 2, *Atmos. Chem. Phys.*, 13, 11019-11058, 10.5194/acp-13-11019-2013, 2013.
- Kuwata, M., Kondo, Y., Mochida, M., Takegawa, N., and Kawamura, K.: Dependence of CCN activity of less volatile particles on the amount of coating observed in Tokyo, *Journal of Geophysical Research: Atmospheres*, 112, 10.1029/2006jd007758, 2007.
- Laakso, L., Grönholm, T., Rannik, Ü., Kosmale, M., Fiedler, V., Vehkamäki, H., and Kulmala, M.: Ultrafine particle scavenging coefficients calculated from 6 years field measurements, *Atmos. Environ.*, 37, 3605-3613, [https://doi.org/10.1016/S1352-2310\(03\)00326-1](https://doi.org/10.1016/S1352-2310(03)00326-1), 2003.
- Lamb, K. D., Perring, A. E., Samset, B., Peterson, D., Davis, S., Anderson, B. E., Beyersdorf, A., Blake, D. R., Campuzano-Jost, P., Corr, C. A., Diskin, G. S., Kondo, Y., Moteki, N., Nault, B. A., Oh, J., Park, M., Pusede, S. E., Simpson, I. J., Thornhill, K. L., Wisthaler, A., and Schwarz, J. P.: Estimating Source Region Influences on Black Carbon Abundance, Microphysics, and Radiative Effect Observed Over South Korea, *J. Geophys. Res. Atmos.*, 123, 527-513, 548, doi:10.1029/2018JD029257, 2018.
- Lee, Y. H., Lamarque, J. F., Flanner, M. G., Jiao, C., Shindell, D. T., Berntsen, T., Bisiaux, M. M., Cao, J., Collins, W. J., Curran, M., Edwards, R., Faluvegi, G., Ghan, S., Horowitz, L. W., McConnell, J. R., Ming, J., Myhre, G., Nagashima, T., Naik, V., Rumbold, S. T., Skeie, R. B., Sudo, K., Takemura, T., Thevenon, F., Xu, B., and Yoon, J. H.: Evaluation of preindustrial to present-day black carbon and its albedo forcing from Atmospheric Chemistry and Climate Model Intercomparison Project (ACCMIP), *Atmos. Chem. Phys.*, 13, 2607-2634, 10.5194/acp-13-2607-2013, 2013.
- Li, M., Zhang, Q., Kurokawa, J. I., Woo, J. H., He, K., Lu, Z., Ohara, T., Song, Y., Streets, D. G., Carmichael, G. R., Cheng, Y., Hong, C., Huo, H., Jiang, X., Kang, S., Liu, F., Su, H., and Zheng, B.: MIX: a mosaic Asian anthropogenic emission inventory under the international collaboration framework of the MICS-Asia and HTAP, *Atmos. Chem. Phys.*, 17, 935-963, 10.5194/acp-17-935-2017, 2017.
- Li, S., Park, S., Park, M.-K., Jo, C. O., Kim, J.-Y., Kim, J.-Y., and Kim, K.-R.: Statistical Back Trajectory Analysis for Estimation of CO₂ Emission Source Regions, *Atmosphere*, 24, 245-251, 2014 (Abstract in English).
- Liu, D., Joshi, R., Wang, J., Yu, C., Allan, J. D., Coe, H., Flynn, M. J., Xie, C., Lee, J., Squires, F., Kotthaus, S., Grimmond, S., Ge, X., Sun, Y., and Fu, P.: Contrasting physical properties of black carbon in urban Beijing between winter and summer, *Atmos. Chem. Phys.*, 19, 6749-6769, 10.5194/acp-19-6749-2019, 2019.
- Liu, L., Zhang, J., Xu, L., Yuan, Q., Huang, D., Chen, J., Shi, Z., Sun, Y., Fu, P., Wang, Z., Zhang, D., and Li, W.: Cloud scavenging of anthropogenic refractory particles at a mountain site in North China, *Atmos. Chem. Phys.*, 18, 14681-14693, 10.5194/acp-18-14681-2018, 2018.
- Lund, M. T., Berntsen, T. K., and Samset, B. H.: Sensitivity of black carbon concentrations and climate impact to aging and scavenging in OsloCTM2–M7, *Atmos. Chem. Phys.*, 17, 6003-6022, 10.5194/acp-17-6003-2017, 2017.
- Luo, G., Yu, F., and Schwab, J.: Revised treatment of wet scavenging processes dramatically improves GEOS-Chem 12.0.0 simulations of surface nitric acid, nitrate, and ammonium over the United States, *Geosci. Model Dev.*, 12, 3439-3447, 10.5194/gmd-12-3439-2019, 2019.
- Matsui, H., Koike, M., Kondo, Y., Moteki, N., Fast, J. D., and Zaveri, R. A.: Development and validation of a black carbon mixing state resolved three-dimensional model: Aging processes and radiative impact, *J. Geophys. Res. Atmos.*, 118, 2304-2326, 10.1029/2012jd018446, 2013.
- Matsui, H., Hamilton, D. S., and Mahowald, N. M.: Black carbon radiative effects highly sensitive to emitted particle size when resolving mixing-state diversity, *Nature Communications*, 9, 3446, 10.1038/s41467-018-05635-1, 2018.
- Miyakawa, T., Oshima, N., Taketani, F., Komazaki, Y., Yoshino, A., Takami, A., Kondo, Y., and Kanaya, Y.: Alteration of the size distributions and mixing states of black carbon through transport in the boundary layer in east Asia, *Atmos. Chem. Phys.*, 17, 5851-5864, 10.5194/acp-17-5851-2017, 2017.
- Mori, T., Kondo, Y., Ohata, S., Moteki, N., Matsui, H., Oshima, N., and Iwasaki, A.: Wet deposition of black carbon at a remote site in the East China Sea, *J. Geophys. Res. Atmos.*, 119, 10485-10498, 10.1002/2014jd022103, 2014.
- Moteki, N., Kondo, Y., Miyazaki, Y., Takegawa, N., Komazaki, Y., Kurata, G., Shirai, T., Blake, D. R., Miyakawa, T., and Koike, M.: Evolution of mixing state of black carbon particles: Aircraft measurements over the western Pacific in March 2004, *Geophysical Research Letters*, 34, 10.1029/2006gl028943, 2007.
- Moteki, N., Kondo, Y., Oshima, N., Takegawa, N., Koike, M., Kita, K., Matsui, H., and Kajino, M.: Size dependence of wet removal of black carbon aerosols during transport from the boundary layer to the free troposphere, *Geophysical Research Letters*, 39, 10.1029/2012gl052034, 2012.



- Myhre, G., Shindell, D., Bréon, F.-M., Collins, W., Fuglestedt, J., Huang, J., Koch, D., Lamarque, J.-F., Lee, D., and Mendoza, B. J. C. c.: Anthropogenic and natural radiative forcing, 423, 658-740, 2013.
- Ogren, J. A., Wendell, J., Andrews, E., and Sheridan, P. J.: Continuous light absorption photometer for long-term studies, *Atmos. Meas. Tech.*, 10, 4805-4818, 10.5194/amt-10-4805-2017, 2017.
- Oh, J., Park, J.-S., Ahn, J.-Y., Choi, J.-S., Lim, J.-H., Kim, H.-J., Han, J.-S., Hong, Y.-D., and Lee, G.-W.: A study on the Behavior of the Black Carbon at Baengnyeong Island of Korea Peninsular, *J. Korean Soc. Urban Environ.*, 14, 67-76, 2014 (Abstract in English).
- Oh, J., Park, J., Lee, S., Ahn, J., Choi, J., Lee, S., Lee, Y., Kim, H., Hong, Y., Hong, J., Kim, J., Kim, S., and Lee, G.-W.: Characteristics of Black Carbon Particles in Ambient Air Using a Single Particle Soot Photometer (SP2) in May 2013, Jeju, Korea, *J. Korean Soc. Atmos.*, 32, 255-268, 2015 (Abstract in English).
- Ohata, S., Kondo, Y., Moteki, N., Mori, T., Yoshida, A., Sinha, P. R., and Koike, M.: Accuracy of black carbon measurements by a filter-based absorption photometer with a heated inlet, *Aerosol Science and Technology*, 53, 1079-1091, 10.1080/02786826.2019.1627283, 2019.
- Oshima, N., Kondo, Y., Moteki, N., Takegawa, N., Koike, M., Kita, K., Matsui, H., Kajino, M., Nakamura, H., Jung, J. S., and Kim, Y. J.: Wet removal of black carbon in Asian outflow: Aerosol Radiative Forcing in East Asia (A-FORCE) aircraft campaign, *J. Geophys. Res. Atmos.*, 117, 10.1029/2011JD016552, 2012.
- Park, J., Song, I., Kim, H., Lim, H., Park, S., Shin, S., Shin, H., Lee, S., and Kim, J.: The Characteristics of Black Carbon of Seoul, *J. Environ. Impact Assess.*, 28, 113-128, 10.14249/EIA.2019.28.2.113, 2019 (Abstract in English).
- Philipp, A., and Seibert, P.: Scavenging and Convective Clouds in the Lagrangian Dispersion Model FLEXPART, in: *Air Pollution Modeling and its Application XXV*, Cham, 2018, 335-340.
- Pisso, I., Sollum, E., Grythe, H., Kristiansen, N. I., Cassiani, M., Eckhardt, S., Arnold, D., Morton, D., Thompson, R. L., Groot Zwaaftink, C. D., Evangelou, N., Sodemann, H., Haimberger, L., Henne, S., Brunner, D., Burkhart, J. F., Fouilloux, A., Brioude, J., Philipp, A., Seibert, P., and Stohl, A.: The Lagrangian particle dispersion model FLEXPART version 10.4, *Geosci. Model Dev.*, 12, 4955-4997, 10.5194/gmd-12-4955-2019, 2019.
- Pryor, S. C., Joerger, V. M., and Sullivan, R. C.: Empirical estimates of size-resolved precipitation scavenging coefficients for ultrafine particles, *Atmos. Environ.*, 143, 133-138, <https://doi.org/10.1016/j.atmosenv.2016.08.036>, 2016.
- Samset, B. H., Myhre, G., Herber, A., Kondo, Y., Li, S. M., Moteki, N., Koike, M., Oshima, N., Schwarz, J. P., Balkanski, Y., Bauer, S. E., Bellouin, N., Bernsten, T. K., Bian, H., Chin, M., Diehl, T., Easter, R. C., Ghan, S. J., Iversen, T., Kirkevåg, A., Lamarque, J. F., Lin, G., Liu, X., Penner, J. E., Schulz, M., Seland, Ø., Skeie, R. B., Stier, P., Takemura, T., Tsigaridis, K., and Zhang, K.: Modelled black carbon radiative forcing and atmospheric lifetime in AeroCom Phase II constrained by aircraft observations, *Atmos. Chem. Phys.*, 14, 12465-12477, 10.5194/acp-14-12465-2014, 2014.
- Sparmacher, H., Fülber, K., and Bonka, H.: Below-cloud scavenging of aerosol particles: Particle-bound radionuclides—Experimental, *Atmospheric Environment. Part A. General Topics*, 27, 605-618, [https://doi.org/10.1016/0960-1686\(93\)90218-N](https://doi.org/10.1016/0960-1686(93)90218-N), 1993.
- Stohl, A., Forster, C., Frank, A., Seibert, P., and Wotawa, G.: Technical note: The Lagrangian particle dispersion model FLEXPART version 6.2, *Atmos. Chem. Phys.*, 5, 2461-2474, 10.5194/acp-5-2461-2005, 2005.
- Textor, C., Schulz, M., Guibert, S., Kinne, S., Balkanski, Y., Bauer, S., Bernsten, T., Berglen, T., Boucher, O., Chin, M., Dentener, F., Diehl, T., Easter, R., Feichter, H., Fillmore, D., Ghan, S., Ginoux, P., Gong, S., Grini, A., Hendricks, J., Horowitz, L., Huang, P., Isaksen, I., Iversen, I., Kloster, S., Koch, D., Kirkevåg, A., Kristjansson, J. E., Krol, M., Lauer, A., Lamarque, J. F., Liu, X., Montanaro, V., Myhre, G., Penner, J., Pitari, G., Reddy, S., Seland, Ø., Stier, P., Takemura, T., and Tie, X.: Analysis and quantification of the diversities of aerosol life cycles within AeroCom, *Atmos. Chem. Phys.*, 6, 1777-1813, 10.5194/acp-6-1777-2006, 2006.
- Ueda, S., Nakayama, T., Taketani, F., Adachi, K., Matsuki, A., Iwamoto, Y., Sadanaga, Y., and Matsumi, Y.: Light absorption and morphological properties of soot-containing aerosols observed at an East Asian outflow site, Noto Peninsula, Japan, *Atmos. Chem. Phys.*, 16, 2525-2541, 10.5194/acp-16-2525-2016, 2016.
- Wang, Q., Jacob, D. J., Spackman, J. R., Perring, A. E., Schwarz, J. P., Moteki, N., Marais, E. A., Ge, C., Wang, J., and Barrett, S. R. H.: Global budget and radiative forcing of black carbon aerosol: Constraints from pole-to-pole (HIPPO) observations across the Pacific, *Journal of Geophysical Research: Atmospheres*, 119, 195-206, 10.1002/2013jd020824, 2014a.
- Wang, X., Zhang, L., and Moran, M. D.: Development of a new semi-empirical parameterization for below-cloud scavenging of size-resolved aerosol particles by both rain and snow, *Geosci. Model Dev.*, 7, 799-819, 10.5194/gmd-7-799-2014, 2014b.
- Winiger, P., Andersson, A., Eckhardt, S., Stohl, A., and Gustafsson, Ö.: The sources of atmospheric black carbon at a European gateway to the Arctic, *Nature Communications*, 7, 12776, 10.1038/ncomms12776, 2016.
- Xu, D., Ge, B., Wang, Z., Sun, Y., Chen, Y., Ji, D., Yang, T., Ma, Z., Cheng, N., Hao, J., and Yao, X.: Below-cloud wet scavenging of soluble inorganic ions by rain in Beijing during the summer of 2014, *Environmental Pollution*, 230, 963-973, <https://doi.org/10.1016/j.envpol.2017.07.033>, 2017.
- Xu, J., Zhang, J., Liu, J., Yi, K., Xiang, S., Hu, X., Wang, Y., Tao, S., and Ban-Weiss, G.: Influence of cloud microphysical processes on black carbon wet removal, global distributions, and radiative forcing, *Atmos. Chem. Phys.*, 19, 1587-1603, 10.5194/acp-19-1587-2019, 2019.
- Zheng, B., Tong, D., Li, M., Liu, F., Hong, C., Geng, G., Li, H., Li, X., Peng, L., Qi, J., Yan, L., Zhang, Y., Zhao, H., Zheng,



- Y., He, K., and Zhang, Q.: Trends in China's anthropogenic emissions since 2010 as the consequence of clean air actions, *Atmos. Chem. Phys.*, 18, 14095-14111, [10.5194/acp-18-14095-2018](https://doi.org/10.5194/acp-18-14095-2018), 2018.
- Zhu, C., Kanaya, Y., Yoshikawa-Inoue, H., Irino, T., Seki, O., and Tohjima, Y.: Sources of atmospheric black carbon and related carbonaceous components at Rishiri Island, Japan: The roles of Siberian wildfires and of crop residue burning in China, *Environmental Pollution*, 247, 55-63, <https://doi.org/10.1016/j.envpol.2019.01.003>, 2019.
- Zikova, N., and Zdimal, V.: Precipitation scavenging of aerosol particles at a rural site in the Czech Republic, *Tellus B: Chemical and Physical Meteorology*, 68, 27343, [10.3402/tellusb.v68.27343](https://doi.org/10.3402/tellusb.v68.27343), 2016.

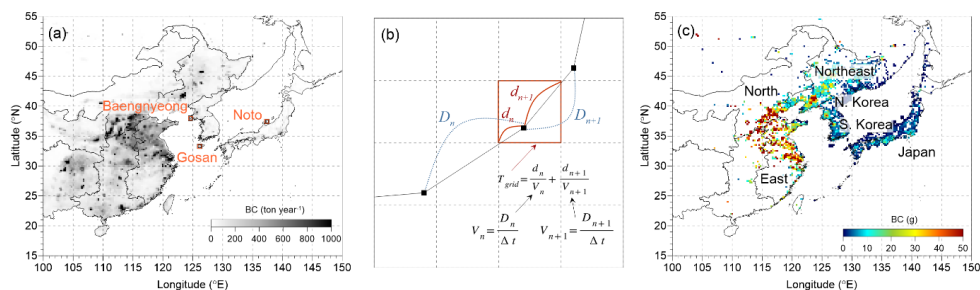


Figure 1. (a) The location of three measurement sites (Baengnyeong, Gosan, and Noto) and the black carbon (BC) emission rate (ton year^{-1}) over East Asia from the Regional Emission inventory in ASia (REAS) version 2.1 (Kurokawa et al., 2013). (b) Illustration of residence time calculated based on the HYSPLIT backward trajectory that passed over a single grid cell (see details in the manuscript). (c) The spatial distribution of the mean BC mass in the potential emission region, which is the highest BC mass grid of each trajectory. The BC mass was obtained by multiplying (a) the emission rates and (b) the residence time.

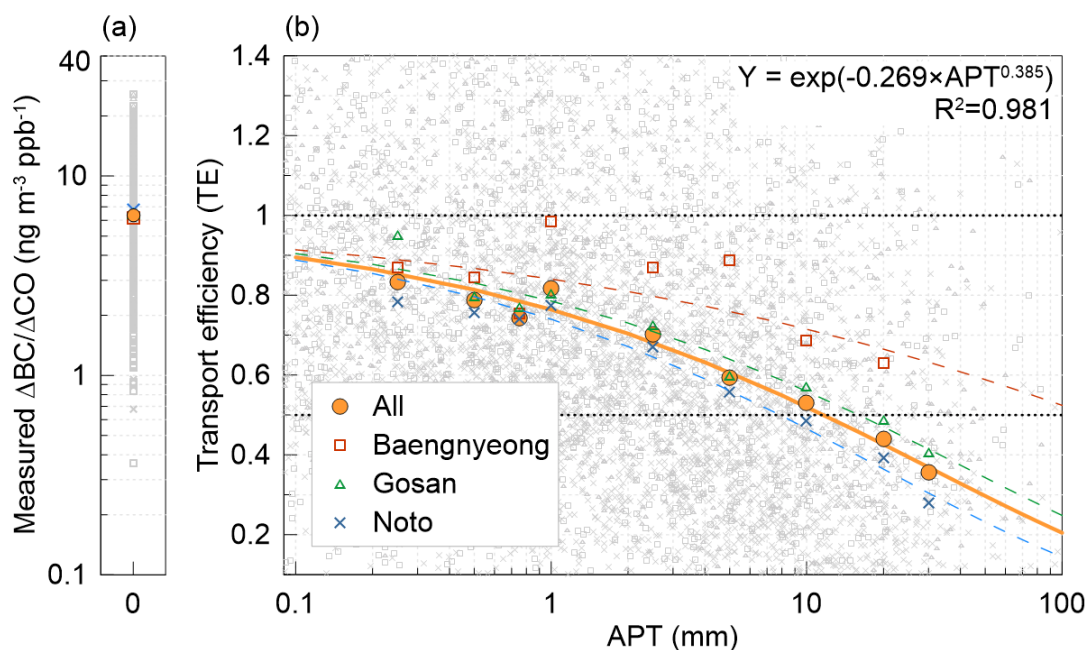


Figure 2. Measured $\Delta BC/\Delta CO$ ratios when accumulated precipitation along trajectory (APT) was zero (left panel) and transport efficiency (TE) variation as a function of APT (right panel) depending on the different sites and overall cases. All data (gray with different symbols) and 9 bins sorted by APT (different colored symbols) are shown. The horizontal dotted lines indicate TE at 0.5 and 1, respectively.

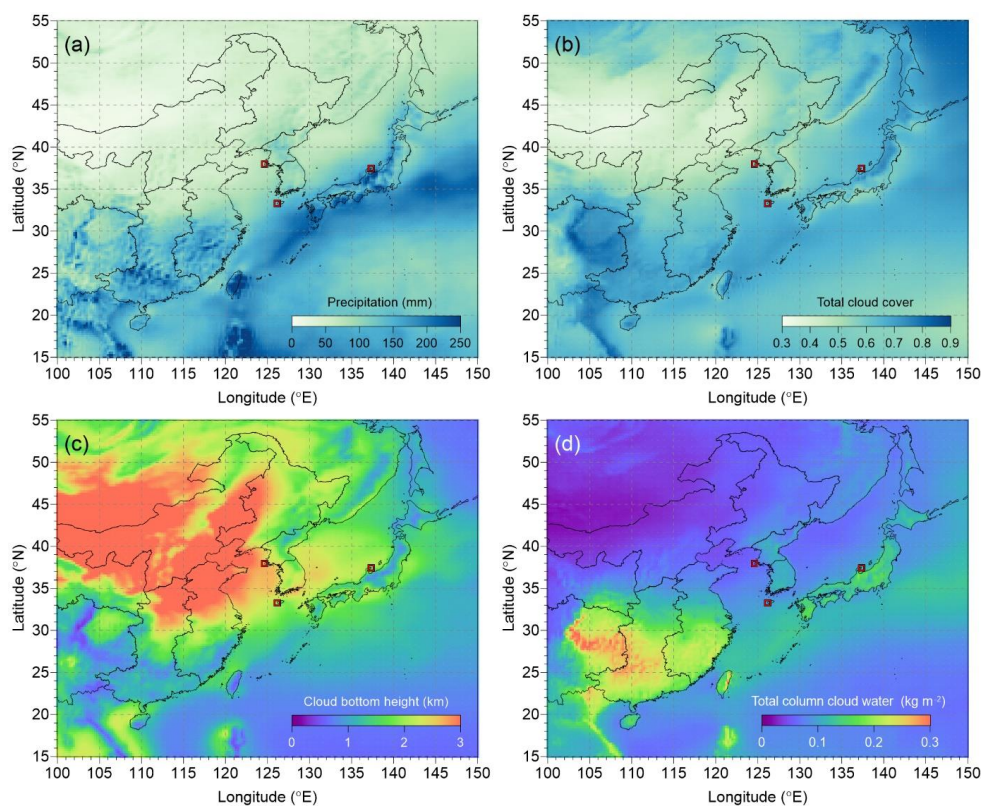


Figure 3. Monthly mean meteorological fields over East Asia from 2010 to 2016 derived from the European Centre for Medium-Range Weather Forecasts (ECMWF) ERA5 monthly averaged data at single levels, (a) precipitation (mm), (b) total cloud cover, (c) cloud bottom height (km), and (d) total column cloud total water (ice and liquid).

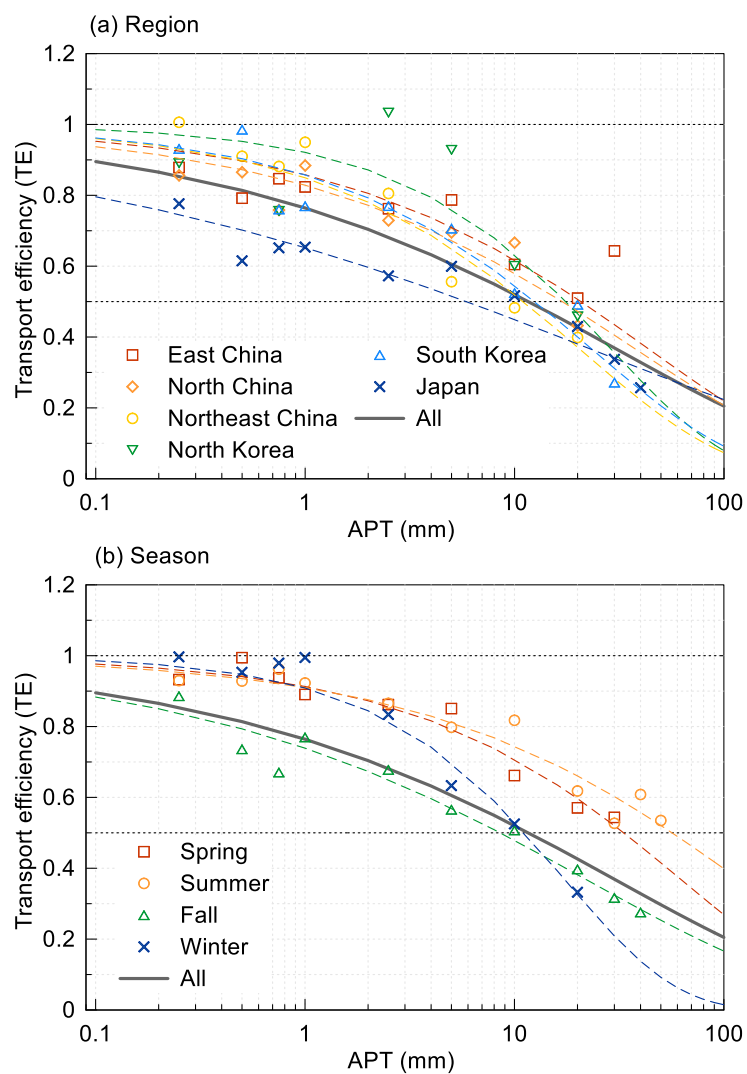


Figure 4. Same as Figure 2 except for (a) regional and (b) seasonal variation of TE according to APT. Each colored symbol and dashed line indicate the different regions and seasons and fitting lines according to stretched exponential decay (SED). The thick gray line depicts the overall fitting line. The horizontal dotted lines indicate TE at 0.5 and 1, respectively.

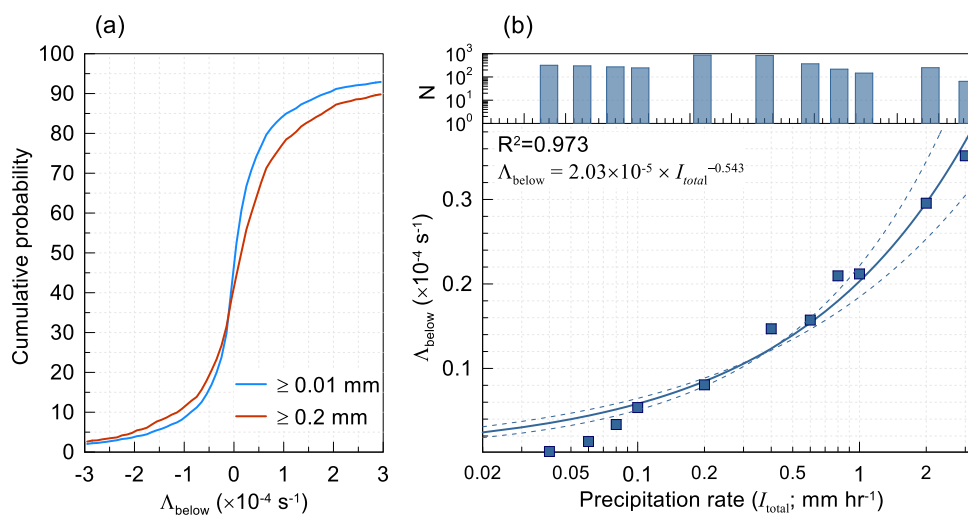


Figure 5. (a) Empirical cumulative distribution plot of measured below-cloud scavenging coefficients (Λ_{below} ; s^{-1}) depending on the precipitation rate (≥ 0.01 and $\geq 0.2 \text{ mm hr}^{-1}$). (b) Median measured Λ_{below} as a function of the precipitation intensity (mm hr^{-1}) of 11 bins. The dashed line indicates the fit from the equation. The upper panel of (b) shows the number of hourly data points for each bin for I_{total} .

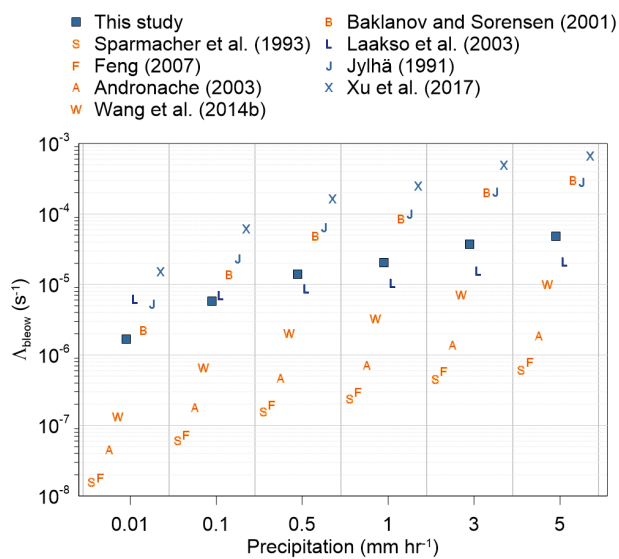


Figure 6. Variation of reported and measured below-cloud scavenging coefficients (Λ_{below} ; s^{-1}) depending on the precipitation intensity (mm hr^{-1}). Orange and blue symbols depict the Λ_{below} equation based on theoretical calculation and observation data, respectively. The diameter of BC was assumed to be approximately 200 nm in the calculation.

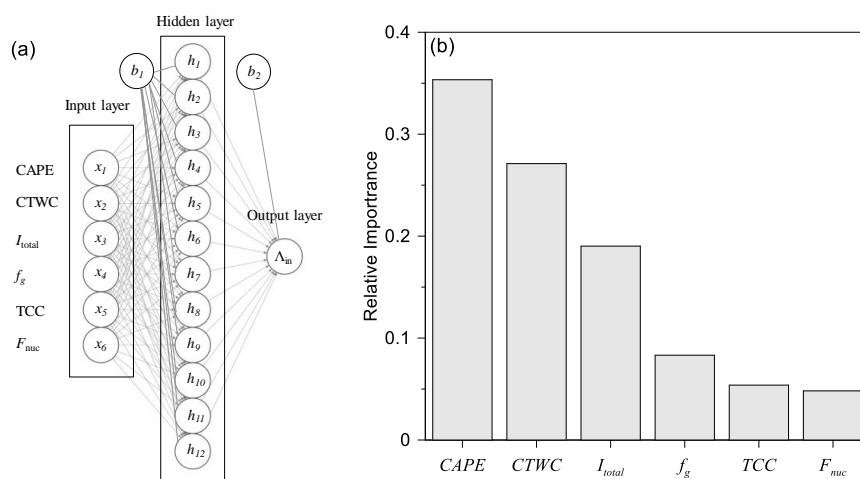


Figure 7. (a) Schematic of an artificial neuron network (ANN) model with 12 nodes of a single hidden layer. (b) The relative importance of six input meteorological variables used for calculating in-cloud scavenging coefficients in the FLEXPART model (except for CAPE) using Garson's algorithm implemented in the 'NeuralNetTools' package in R. CAPE, CTWC, I_{total} , f_g , TCC, and F_{nuc} represent the convective available potential energy, specific cloud total water content, precipitation rate, fraction of a subgrid in a grid cell (see manuscript for details), total cloud cover, and nucleation efficiency, respectively.



Table 1. Summary of the relationship between transport efficiency (TE) and accumulated precipitation along trajectory (APT) in Figures 2 and 4.

	Fitting parameters ^a		R ²	APT (mm)		Number of data points		Days		Annual Precipitation (mm)
	A ₁	A ₂		TE=0.5	TE=1/e	N _{APT=0}	N _{APT>0} ^b	TE=0.5	TE=1/e	
All	0.269 ± 0.039	0.385 ± 0.035	0.981	11.7	30.2	3,565	6,611	2.8	7.1	1542.3
Site										
Baengnyeong	0.156 ± 0.117	0.350 ± 0.146	0.773	70.9	201.9	1,732	1,522	35.5	101.2	728.3
Gosan	0.235 ± 0.047	0.386 ± 0.047	0.964	16.4	42.3	705	1,090	4.9	12.5	1233.3
Noto	0.306 ± 0.052	0.393 ± 0.036	0.985	8.0	20.3	1,128	4,057	1.1	2.8	2665.3
Region										
East	0.153 ± 0.099	0.498 ± 0.183	0.866	20.7	43.3	439	704			
North	0.188 ± 0.090	0.462 ± 0.175	0.897	16.9	37.3	518	495			
Northeast	0.163 ± 0.084	0.603 ± 0.166	0.945	11.0	20.3	1,237	2,175			
N. Korea	0.082 ± 0.414	0.745 ± 0.813	0.656	17.5	28.7	216	393			
S. Korea	0.154 ± 0.110	0.596 ± 0.188	0.922	12.5	23.2	325	680			
Japan	0.428 ± 0.117	0.272 ± 0.089	0.925	5.9	22.6	687	1,789			
Season										
Spring	0.122 ± 0.045	0.506 ± 0.111	0.957	31.2	64.5	1,285	1,366			
Summer	0.143 ± 0.107	0.362 ± 0.182	0.780	77.3	212.6	497	1,685			
Fall	0.288 ± 0.055	0.397 ± 0.057	0.972	9.1	23.0	767	1,606			
Winter	0.070 ± 0.048	0.905 ± 0.192	0.964	12.5	18.7	1,016	1,986			

^a TE = exp(-A₁ × APT^{A₂})

^b The number of satisfactory data points in each bin relative to total N_{APT>0} ≥ 2%



Table 2. Summaries of the transport efficiency (TE) and scavenging coefficients for selected (a) below- and (b) in-cloud cases based on ERA5 hourly data of pressure levels from ECMWF.

Cases	Median	Interquartile range (25 th percentile – 75 th percentile)
(a) Below cloud ($N_{case} = 831$)		
TE	0.89	[0.61 – 1.27]
Estimated Λ_{below} (s^{-1})	4.01×10^{-6}	$[2.70 \times 10^{-6} - 6.33 \times 10^{-6}]$
FLEXPART Λ_{below} (s^{-1})	6.63×10^{-6}	$[6.38 \times 10^{-6} - 7.08 \times 10^{-6}]$
(b) In-cloud ($N_{case} = 769$)		
TE	0.72	[0.43 – 1.06]
Estimated Λ_{in}^* (s^{-1}) ^a	8.06×10^{-5}	-
FLEXPART Λ_{in}^* (s^{-1}) ^a	7.28×10^{-6}	-

^{a)} Overall median value